Performance Evaluation of SiC-based Isolated Bidirectional DC/DC Converters for Electric Vehicle Charging

Kaushik Naresh Kumar[*], Rafał Miśkiewicz[#], Przemysław Trochimiuk[#], Jacek Rąbkowski[#], Dimosthenis Peftitsis[*]
[*]NORWEGIAN UNIVERSITY OF SCIENCE AND TECHNOLOGY, Department of Electric Power Engineering, Trondheim, Norway
[#]WARSAW UNIVESITY OF TECHNOLOGY, Institute of Control and Industrial Electronics, Warsaw, Poland
E-Mail: kaushik.n.kumar@ntnu.no, rafal.miskiewicz@pw.edu.pl, przemyslaw.trochimiuk@pw.edu.pl, jacek.rabkowski@pw.edu.pl, dimosthenis.peftitsis@ntnu.no

Acknowledgements

This work is supported by the "Modularized, Reconfigurable and Bidirectional Charging Infrastructure for Electric Vehicles with Silicon Carbide Power Electronics" (MoReSiC) project, funded by the POLNOR programme in the Norway-Poland EEA Grants framework.

Keywords

«Dual Active Bridge (DAB)», «DC-DC converters», «Electric vehicle (EV) charging», «Silicon Carbide (SiC) MOSFET»

Abstract

In this paper, six 10 kW DC/DC isolated and bidirectional dual active bridge topologies, supplied by +750/0/-750V three-wire DC bus, are evaluated based on efficiency, loss distribution, volt-ampere semiconductors ratings and normalized cost of SiC MOSFETs for electric vehicle charging applications. The selected topologies are evaluated under the same voltage and power conditions, through electrothermal simulations and experiments. The simulation results were verified through experiments conducted on 5 kW prototypes of four of the considered topologies. The advantages and disadvantages of the topologies are discussed and analyzed based on the chosen performance metrics. It has been shown that series-resonant input-series output-parallel full-bridge DAB topology exhibits the highest efficiency while the active neutral point clamped (ANPC) DAB topology can be designed with the lowest cost. However, considering a fair trade-off between all the performance metrics, series-resonant ANPC DAB topology is shown to be the best design choice for the considered evaluation conditions.

1. Introduction

Electrification of the transportation sector plays a key role in the decarbonization of the environment. In this context, the installation of advanced electric vehicles (EVs) fast charging infrastructure with bidirectional capability is paramount considering challenges like EVs demand flexibility, power grid support, etc. [1]. The isolated bidirectional DC/DC converter (IBDC) is one of the key components of such an EV charging system and the first step for its design is the choice and performance evaluation of the utilized power electronics converter topology.

The advantages of dual active bridge (DAB) topology introduced in [2] are its soft-switching capability, higher power density, galvanic isolation, bidirectional power flow capability, and wide voltage gain range [3]. Silicon Carbide (SiC) metal oxide semiconductor field-effect transistors (MOSFETs) can switch at higher frequencies, block higher voltages for the same conduction loss performance, and operate at higher temperatures compared to Silicon insulated gate bipolar transistors (IGBTs) [4] [5]. It is inferred from other EV applications that employing SiC power devices may be highly beneficial in

terms of efficiency and compactness [6] [7] [8]. Therefore, DAB topologies employing SiC MOSFETs are evaluated in this paper. The EV charging system considered in this evaluation is based on bipolar (three-wire) DC bus as depicted in Fig. 1. The advantages of using a bipolar DC bus include lower on-state losses in devices, higher power quality and enhanced flexibility [9] [10] [11].

Comparison of IBDC DAB converter topologies employing wide band gap (WBG) devices have been presented for applications such as EV fast chargers [12], more electric aircraft [13] and other power applications [14]. However, there is not much literature available for such a comparison considering an EV charging system using bipolar DC bus with appropriate experimental validation. In this point of view, the contribution of this work is on the performance evaluation of various IBDC DAB converter topologies through electrothermal modeling and simulation, as well as laboratory prototyping and experimental validation. The paper is organized as follows: Section 2 presents the topologies under investigation and their design considerations. In Section 3, the performance of the topologies based on volt-ampere ratings, normalized cost, efficiency, and loss distribution of SiC MOSFETs is evaluated using theoretical analysis and simulations. Section 4 provides a description of the experimental prototypes and the results from experiments are summarized and compared to simulation results in Section 5. Section 6 presents the conclusion.

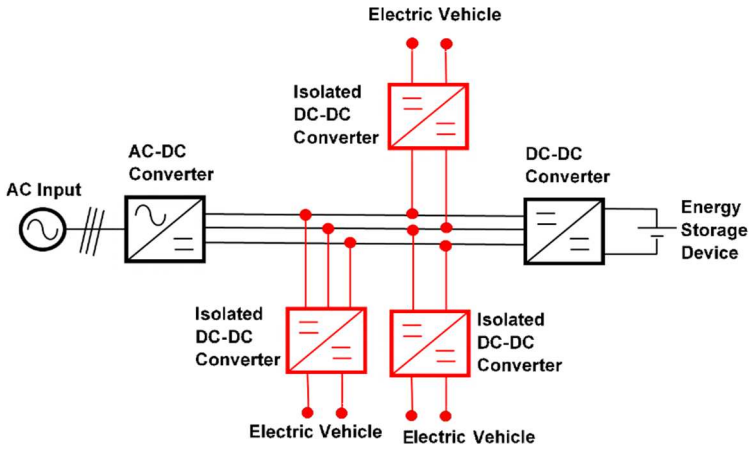

Fig. 1: Schematic of the EV Charging system based on bipolar DC bus.

2. Evaluated DAB-based topologies

DAB-based IBDC generally consists of two full-bridge (FB) circuits that are galvanically isolated by means of a high frequency transformer. For positive power flow, the primary FB operates as an inverter and the secondary FB functions as a rectifier. In the traditional single-phase-shift (SPS) modulation, the switches in both FBs operate at 50% fixed duty ratio and generate high frequency AC square-wave voltages across the transformer primary and secondary sides. The direction and magnitude of transferred power can be controlled by the phase difference between the FBs like conventional ac power systems.

Considering the bipolar (three-wire) nature of the DC bus and the two-terminal nature of EV battery load, two fundamental circuits for the isolated DAB converters have been chosen, namely, the full-bridge (FB) and the active neutral-point clamped (ANPC) circuits, as shown in Figs. 2(d) and (e), respectively. These circuits can be combined for designing either one-to-one isolated DAB converters comprising a single primary bridge and single secondary bridge or multiport counterparts. Fig. 2(c) depicts a one-to-one isolated DAB topology employing an ANPC circuit on the primary side and a FB circuit on the secondary side that are coupled though a high-frequency transformer.

To increase the flexibility in terms of voltage and electric power supplied, the FB and ANPC circuits can be connected in series or in parallel. The input-series output-parallel (ISOP) configuration is one such topology that provides voltage flexibility on the primary side through series-connected circuits and power scalability in the secondary side through parallel-connected circuits. Fig. 2(a) shows an ISOP FB DAB topology where the series-connected primary and parallel-connected secondary bridges consist of FB circuit. Fig. 2(b) depicts an ISOP ANPC DAB topology with series-connected ANPC circuit on the

primary side and parallel-connected FB circuits on the secondary side. Both series-resonant (SR) and non-resonant variants of each of the three listed topologies are evaluated to study their performance, as well as advantages and disadvantages. Topologically, the SR DAB configurations require an additional capacitor to form a L_rC_r resonant tank (shown in blue in Figs. 2(a)-(c)) compared to the non-resonant DAB converters, which only have a series-inductance, L (shown in green in Figs. 2(a)-(c)). The series-inductance represents the sum of the transformer leakage inductance plus any external and parasitic inductance in the circuit.

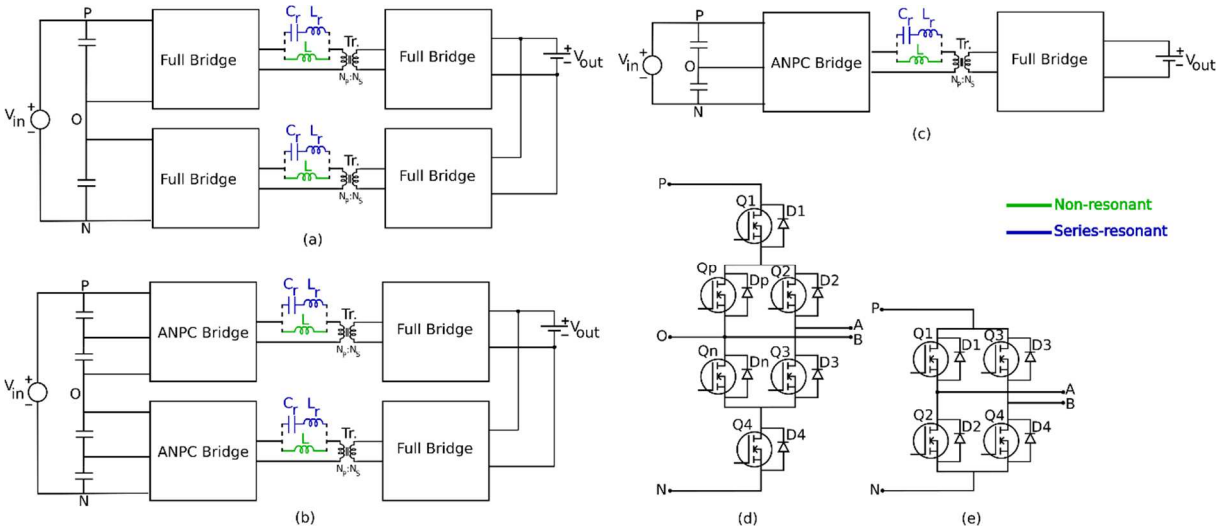

Fig. 2: Block diagrams of the evaluated topologies: (a) ISOP FB DAB, (b) ISOP ANPC DAB, (c) ANPC DAB, (d) ANPC bridge, and (e) Full bridge.

2.1. Design considerations

The selected topologies depicted in Fig. 2 are evaluated under the same voltage and power levels. The values considered for the dc input voltage (V_{in}), dc output voltage (V_{out}), output power (P_{out}), switching frequency (f_{sw}), non-resonant/resonant series-inductance (L/L_r), resonant capacitance (C_r), and transformer turns ratio (N) are summarized in Table I.

Table I: Design parameters for the converters.

DAB type	Non-resonant DAB	Series-resonant DAB
V_{in}	1500V	
V_{out}	400 V	
P_{out}	10 kW	
f_{sw}	100 kHz	
L/L_r	17µH – 70µH*	100 µH
C_r	-	28 nF
N	$V_{primary\_pk}/V_{secondary\_pk}$	

$V_{primary\_pk}$ - peak transformer primary voltage

$V_{secondary\_pk}$ - peak transformer secondary voltage

*Calculated using Eqn.2 depending on topology

Table II: SiC MOSFETs utilized in each topology

Topology	MOSFET used in primary bridge	MOSFET used in secondary bridge
ISOP FB DAB	NTH4L040N120SC1[1]	C3M0015065K[2]
ISOP ANPC DAB	IMZA65R039M1HXKSA1[3]	C3M0015065K[2]
ANPC DAB	NTH4L040N120SC1[1]	C3M0015065K[3]

[1]1200V, 40mΩ, 58A SiC MOSFET from ON semiconductor

[2]650V, 15mΩ,120A SiC MOSFET from CREE

[3]650V, 39mΩ, 50A SiC MOSFET from Infineon

The switching frequency, f_{sw} is chosen to be 100 kHz as a fair trade-off between the heat sink size, the size of magnetics and the switching losses. The selection of SiC MOSFETs was made considering the type of bridge circuit (i.e., ANPC or FB), considered voltage and power levels, better switching performance in terms of faster switching transients due to lower stray inductance in the gate loop (four-pin devices with Kelvin connection) and their availability in the market. Table II summarizes the chosen SiC MOSFETs for each topology and their ratings.

Since the performance evaluation based on efficiency and losses of SiC MOSFETs are carried out at a specific operating point, only the unidirectional power flow operation of the chosen converter topologies is considered. Therefore, the EV battery is modelled as a resistive load, R_{load} given by:

$$R_{load} = \frac{V_{out}^2}{P_{out}} \tag{1}$$

The power transfer equation for a non-resonant DAB converter operating with SPS modulation is given by:

$$P_{out} = N * V_{primary} * V_{secondary} * \frac{\big(D * (1 - D)\big)}{2 * f_{sw} * L} \tag{2}$$

Where, D is the phase-shift ratio ($0 < D < 1$) between primary and secondary bridges. The value of inductor, L is calculated according to Eqn. 2 for a phase shift of $D = 0.5$ and for twice the nominal power level. The reason for this approach is to ensure lower reflow power at the nominal operating point, where reflow power refers to the power flow back to the source caused by circulating currents in the converter [15]. It is to be noted that the value of L is calculated at P_{out} = 10 kW per each module of the ISOP FB DAB and ISOP ANPC DAB configurations (each module is operated at 5 kW nominal power) and at P_{out} = 20 kW for the ANPC DAB configuration for a nominal operating power of P_{out} = 10 kW.

In the case of resonant DABs, the L_r and C_r values are chosen such that the resonance frequency, f_r is less than the switching frequency, f_{sw} of the converter to ensure continuous current mode operation [16]. The resonance frequency, f_r is given by:

$$f_r = \frac{1}{2 * \pi * \sqrt{L_r * C_r}} \tag{3}$$

The transformer turns ratio, N is chosen to be equal to the ratio of the transformer voltages as given in Table I to ensure zero voltage switching and to reduce the stress on transformer by reducing circulating currents.

3. Performance Evaluation

This section presents the performance evaluation of the topologies under study using theoretical analysis and simulations. In particular, the required volt-ampere ratings of power semiconductors, as well as the loss distribution among the primary and secondary FBs are evaluated based on simulations.

3.1. Evaluation based on Volt-Ampere (VA) rating and normalized cost of SiC MOSFETs

Table III summarizes the SiC MOSFETs' VA ratings and normalized costs for each of the evaluated topologies, where the VA ratings are calculated based on the total number of switches and ratings of the chosen SiC MOSFETs (see Table II).

From Table III, it is seen that the ANPC DAB is the most cost-effective configuration and requires the lowest VA ratings of SiC MOSFETs compared to the ISOP DAB topologies for the considered operating conditions. However, considering the reliability, the ISOP DABs are better compared to the ANPC DAB. This is because the two parallel DAB modules in a ISOP DAB topology share the total power transferred, which decreases the current stress on the switches. In terms of physical components, the series-resonant DABs require an additional resonant capacitance compared to the non-resonant variants

which may contribute to a decrease in power density and an increase in losses due to its equivalent series resistance (ESR).

TABLE III: Summary of VA ratings and normalized costs

Topology	VA rating of SiC MOSFETs (kVA)			Normalized total cost of MOSFETs*
ISOP FB DAB	Primary bridge	Secondary bridge	Total	
	556.8 (8 * 1200V * 58A)	624 (8 * 650V * 120A)	1180.8	2.34
ISOP ANPC DAB	390 (12 * 650V * 50A)	624 (8 * 650V * 120A)	1014	2.32
ANPC DAB	417.6 (6 * 1200V * 58A)	312 (4 * 650V* 120A)	729.6	1.44

*Cost normalized per 200 USD

3.2. Evaluation based on efficiency and MOSFET loss distribution

As all the evaluated topologies are designed to operate at unity voltage transfer ratio and similar voltage and power levels, the major differentiating factor between them is the rating and number of SiC MOSFETs used. Therefore, the efficiency and loss distribution comparison have been performed based only on the SiC MOSFET losses. The calculation of efficiency and losses for the considered topologies is performed in PLECS simulation environment using the corresponding SiC MOSFET models.

Table II contains the information about the MOSFETs types and ratings used in simulations. The SiC MOSFET simulation model for C3M0015065K was provided on the manufacturer's (i.e., Wolfspeed) webpage. The PLECS models for the NTH4L040N120SC1 (from ON semiconductor) and IMZA65R039M1HXKSA1 (from Infineon) were developed using parameters extracted from their respective datasheets and by conducting simulations using their LT SPICE models. LT SPICE models were mainly used for estimation of switching energies. The modelling considerations for the evaluated topologies are as described in Subsection 2.1 and the simulation parameters correspond to Table I.

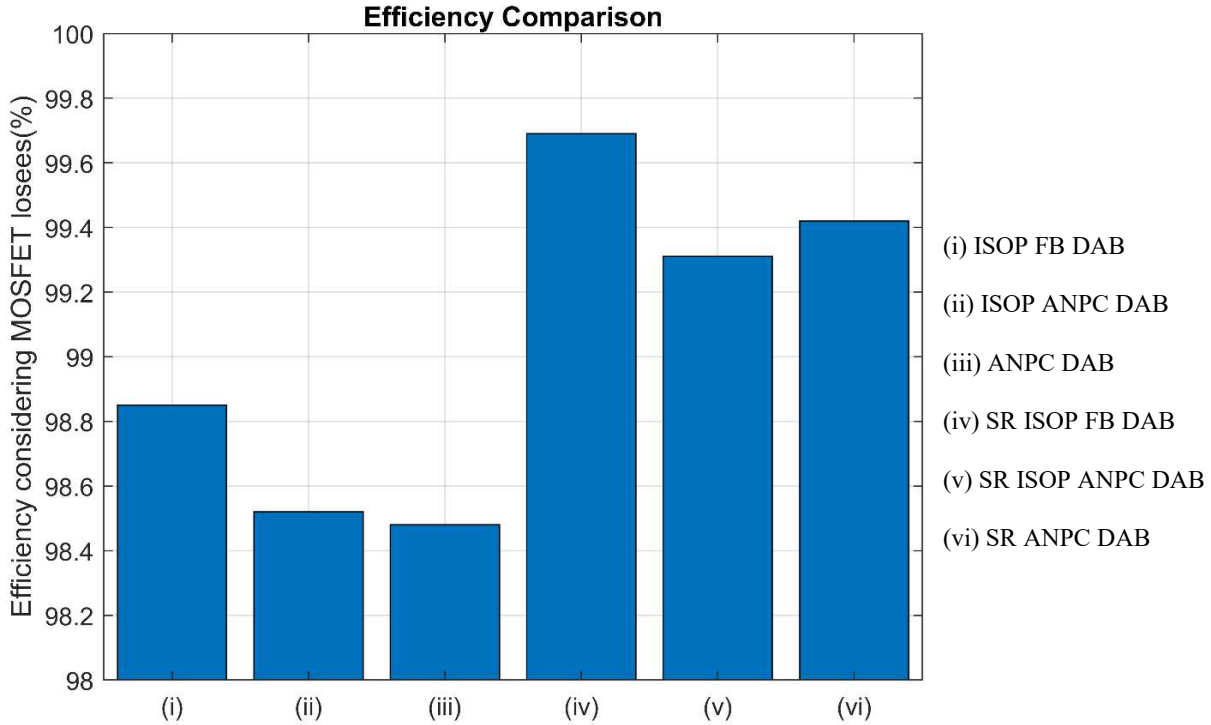

Fig. 3: Comparison of efficiency considering only the MOSFET losses based on simulations.

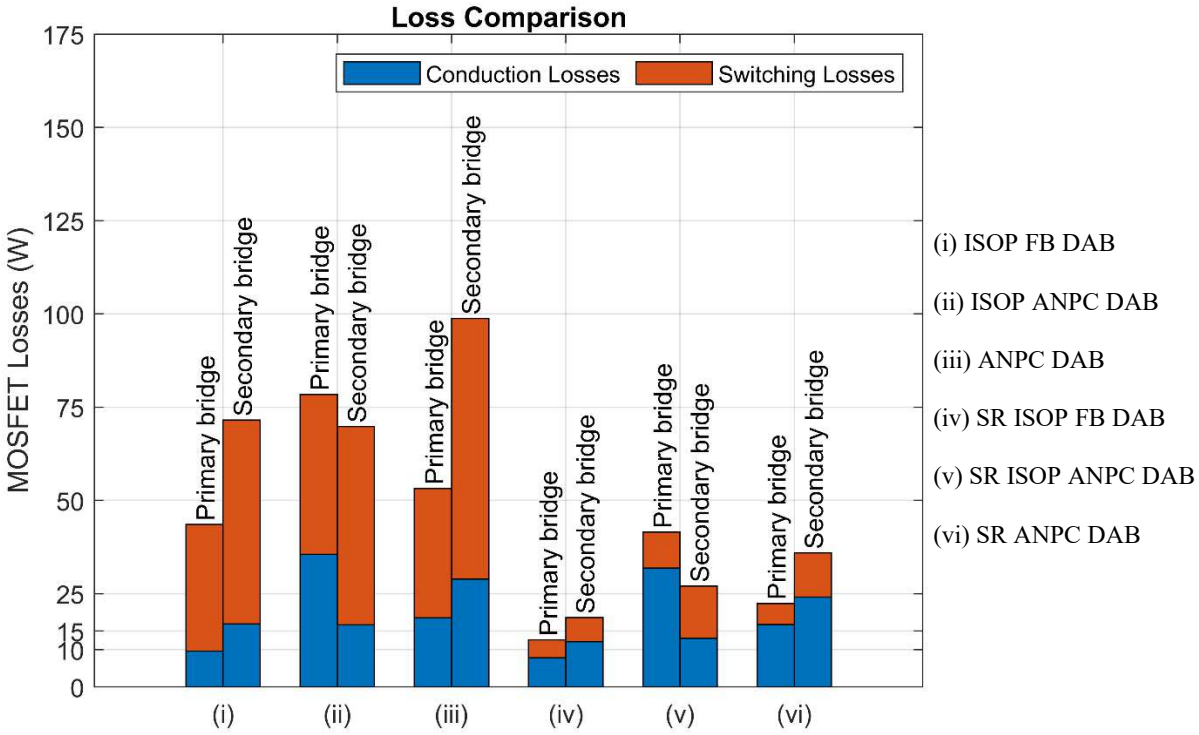

Fig. 4: Comparison of MOSFET loss distribution based on simulations.

In the comparison of efficiency based on MOSFET losses as shown in Fig. 3, the series-resonant DAB configurations outperform the non-resonant variants. One possible reason for the better efficiency of SR variants is due to the operation of SiC MOSFETs near soft switching region in both primary and secondary bridges. This fact is reflected in the MOSFET loss distribution shown in Fig. 4, where the switching losses in both primary and secondary bridges of the SR DABs (i.e., iv, v and vi) are far lower compared to the non-resonant DABs. An additional reason is the sinusoidal shape of the transformer currents in the SR DABs, which results in lower RMS currents and in turn lower conduction losses. This can be observed in Fig. 4, where the conduction losses of the SR DABs are lower in both primary and secondary bridges compared to the respective non-resonant variants.

Among ISOP FB DAB and ISOP ANPC DAB configurations, considering both non-resonant and SR variants, the main difference is the higher conduction losses in the primary bridge for the ISOP ANPC DAB as seen in Figs. 4(ii) and (v). The reason for this is that ISOP ANPC DABs carry almost double the current in the primary bridge compared to ISOP FB DABs for the same power transferred, as only half of the input voltage is reflected on the transformer primary. The higher secondary bridge current (almost double) in non-resonant ANPC DAB compared to the ISOP topologies causes higher switching losses, since the MOSFET switching energy is dependent on drain current. This can be observed in Fig. 4 (iii).

3.3. Evaluation Summary

The spider plot in Fig. 5 summarizes the evaluation of the considered topologies based on the performance metrics discussed in Subsections 3.1 and 3.2. The series-resonant topologies exhibit higher efficiencies compared to their non-resonant variants, which can be attributed to their significantly lower switching losses. The FB topologies exhibit lower conduction losses compared to the ANPC topologies. In terms of VA ratings and normalized cost of SiC MOSFETs, the ANPC DAB topology has a clear advantage compared to the ISOP FB and ISOP ANPC DAB configurations. The SR ANPC DAB topology combines the advantages of both the series-resonant configuration (i.e., lower switching losses and higher efficiency) and the ANPC topology (i.e., lower VA ratings and normalized cost of SiC MOSFETs). This makes it the best design choice for the evaluated application, considering all performance metrics.

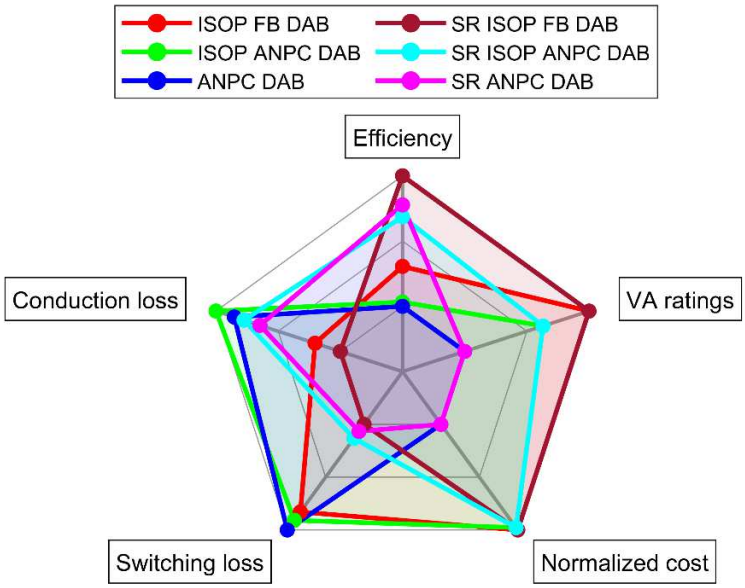

Fig. 5: Comparison of the evaluated topologies based on all the chosen performance metrics.

4. Laboratory prototype

Since the ISOP DAB configuration consists of two parallel-connected DAB modules sharing the total power transferred, validation of a single module is sufficient in terms of efficiency comparison. Therefore, 5 kW prototypes of single modules of non-resonant and series-resonant variants of ISOP FB and ANPC DABs were built-up for the experimental validation of the simulation results. Fig. 6 shows a photo of the non-resonant FB DAB laboratory prototype.

The experimental parameters summarized in Table IV correspond to half the dc input voltage and output power levels considered for simulations (See Table I), since they refer to a single module of non-resonant and SR versions of ISOP FB and ISOP ANPC DABs. The series-inductances values include the stray inductances of transformer windings measured using impedance analyzer. The actual transformer turns ratio for the ANPC configuration was 0.909 as opposed to the calculated value of 0.9375. In case of FB configuration, the calculated transformer turns ratio was achieved. The resonant capacitances have different values for the SR ANPC and FB DABs to keep the resonant frequency the same irrespective of the deviation in the transformer turns ratio and leakage inductances between the two configurations.

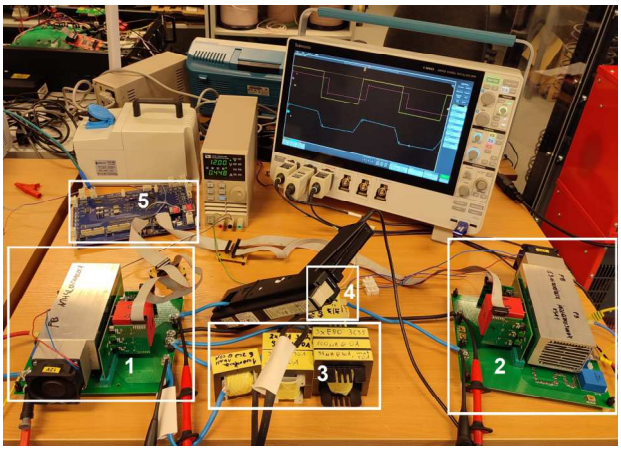

Fig. 6: 5 kW non-resonant FB DAB prototype: (1) Primary full bridge, (2) Secondary full bridge, (3) Series inductor, (4) Transformer, and (5) Control board.

Table IV: Experimental parameters

DAB type	Non-resonant DAB	Series-resonant DAB
V_{in}	750V	
V_{out}	400 V	
P_{out}	5 kW	
f_{sw}	100 kHz	
L/L_r	18.2[a] – 72.5µH[b]	100 µH
C_r	-	26.9[a] – 30.5[b] nF
N	0.909[a] – 1.875[b]	
R_{load}	30.5 Ohms	

[a] ANPC DAB
[b] FB DAB

The efficiency measurements were carried out using the YOKOGAWA WT5000 power analyzer and the transformer current and voltage waveforms were captured using Tektronix DPO 4034 mixed signal oscilloscope for all the DABs. Tektronix THDP0200 high-voltage differential probes were used for voltage measurements. Tektronix TCP0150 and TCP303 current probes were used for current measurements. The YOKOGAWA WT5000 power analyzer has an accuracy of ± (0.1% reading error + 0.1% measurement range error) for voltage, current and power measurements. The accuracy is also influenced by the temperature and aging of the equipment. The interesting observations from the simulations are related to comparison between the non-resonant and series-resonant DABs and the difference between the FB and ANPC configurations. Therefore, only four out of the six topologies considered were tested experimentally.

5. Experimental results

The experimental results consisting of converter efficiency measured in the DC circuit and the transformer voltage and current waveforms in the AC circuit are shown in Figs. 7(a)-(d) for the investigated topologies. In Figs. 7(a) and (b) the voltage per division is 500V and current per division is 10A. In Figs. 7(c) and (d) the voltage per division is 250V and current per division is 25A. It should be noted that the power analyzer data correspond to the overall converter efficiency whereas efficiency due to only MOSFET losses was considered in the simulations.

Most of the observations discussed in Subsection 3.2 can be validated from the experimental results. From Figs. 7(a) and (b) and Figs. 7(c) and (d), it can be observed that the SR DABs have a near sinusoidal transformer current waveform compared to their non-resonant counterparts, resulting in lower RMS bridge currents. From Figs. 7(a) and (c) and Figs. 7(b) and (d) it can be observed that the ANPC DABs carry almost double the current in the primary bridge and reflects half of the DC input voltage on transformer primary compared to FB DABs for the same power transferred.

Due to zero current switching and reduced RMS bridge currents in SR FB DAB as seen in Fig. 7(b), this topology exhibits the lowest losses. One of the reasons for high losses in the SR ANPC DAB can be attributed to hard switching at higher current values (nearly 10A) as seen in Fig. 7(d). Since the calculated value of transformer turns ratio did not match the actual value in the prototype, the zero current switching could not be achieved for the considered operating conditions. This shows the sensitivity of resonant circuits when operating them under practical conditions.

It should be noted that the value of resonant capacitor, C_r in both the SR DAB prototypes was achieved by series connection of two strings of 17 parallel-connected ceramic capacitors. The ESR of each ceramic capacitor at 100 kHz was found to be 2 ohms and the effective ESR of the C_r was estimated to be 0.235 ohms. Since the SR ANPC DAB has a primary RMS current of about 17A compared to 8A in SR FB DAB, the losses due to the ESR of C_r is about 68W and 15W, respectively. This is one of the major contributors to higher losses in the SR ANPC DAB.

Fig. 8 shows a comparison of the efficiency values obtained from the simulations with the experimental results for the investigated topologies. Simulation results are based on only MOSFET losses whereas experimental results correspond to the overall converter's efficiency. The difference between the experimental efficiencies and simulation efficiencies can be attributed to other losses like transformer core and copper losses, losses due to ESR of resonant capacitors, inductor losses, and other resistive losses. It can be observed that the general trend of efficiency data from the simulations agree with experimental results except for the SR ISOP ANPC DAB topology. The reasons for this deviation are as described above. In addition, it should be noted that the simulations were carried out based on calculated values of series-inductance, resonance capacitance and transformer turns-ratio without considering the actual experimental parameters like parasitic inductances, contact resistances, actual transformer turns-ratio and the ESR of resonant capacitor.

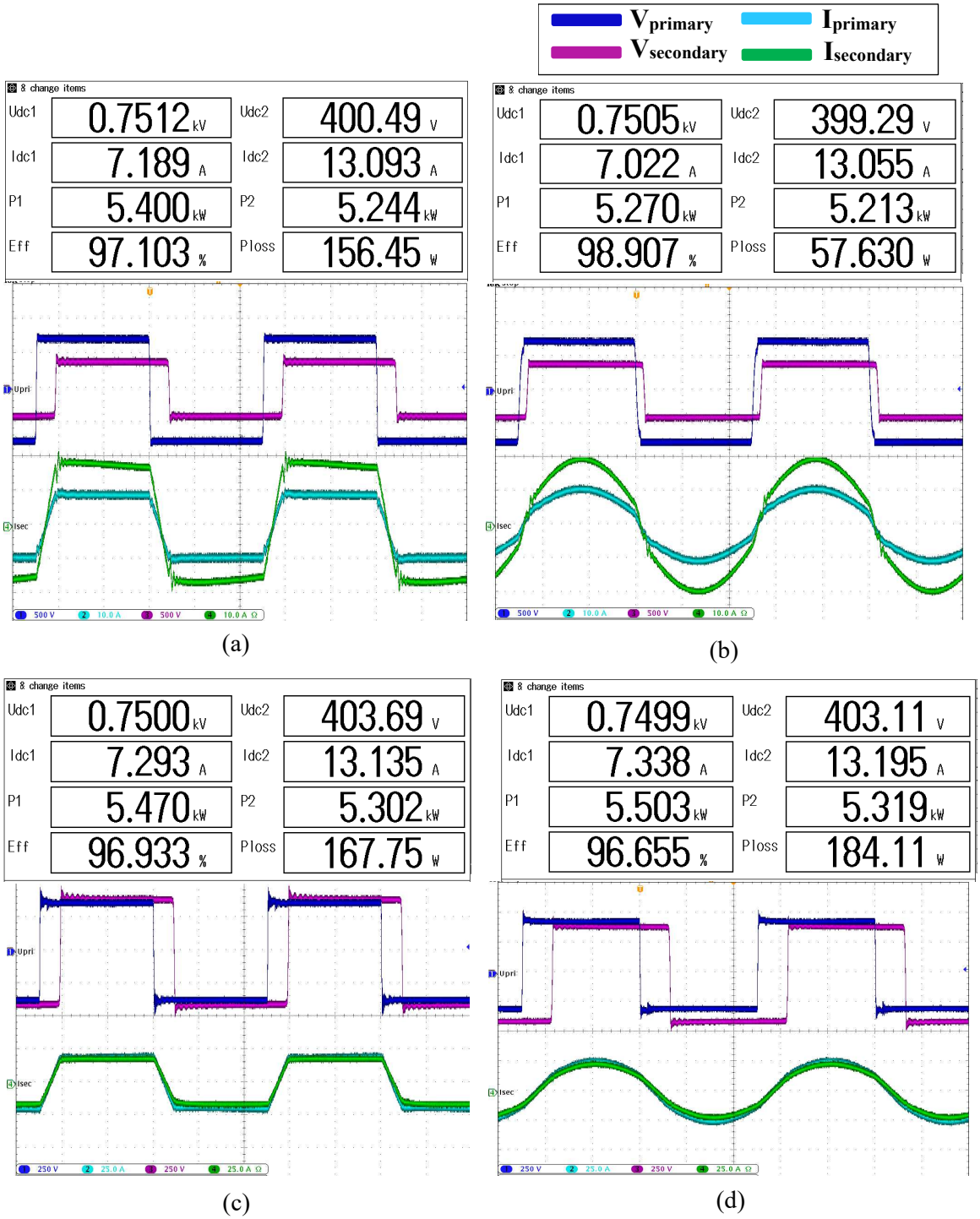

Fig. 7: Experimental results: Power analyzer data and transformer voltage and current waveforms for (a) non-resonant FB DAB, (b) series-resonant FB DAB, (c) non-resonant ANPC DAB and (d) series-resonant ANPC DAB

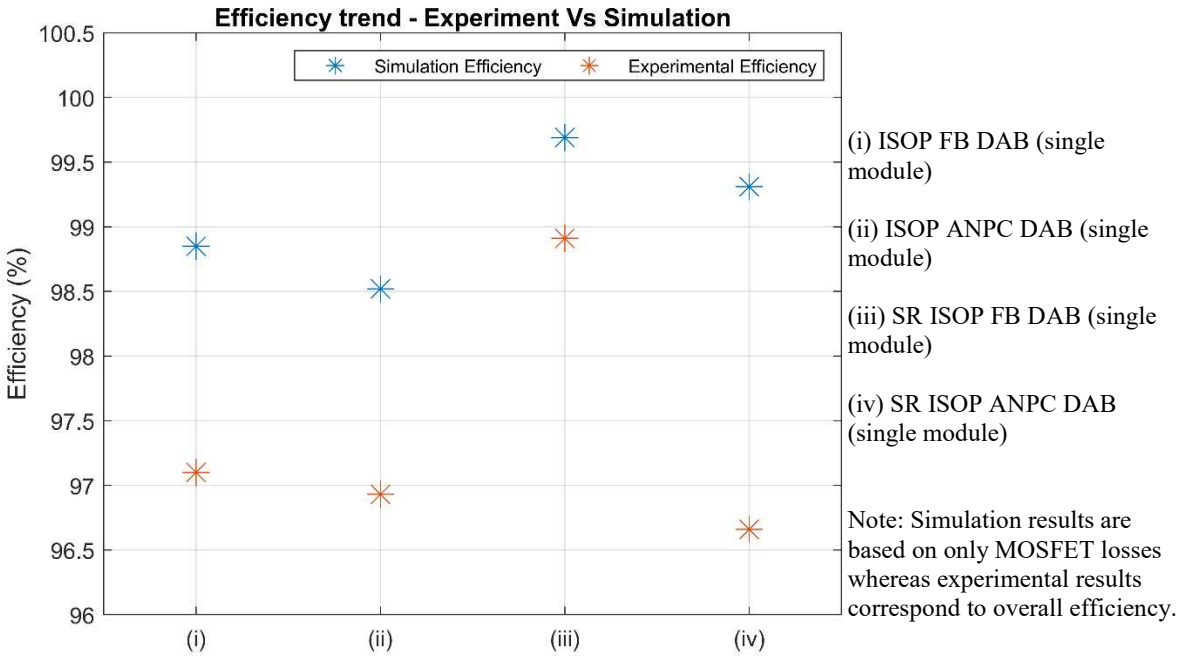

Fig. 8: Comparison of efficiency results from simulations and experiments

6. Conclusions

Six different configurations of the IBDC DAB topology have been evaluated for a 10-kW EV charging application. The topologies were selected considering the bipolar (three-wire) nature of input DC bus, two-terminal nature of EV battery load, flexibility of voltage as well as power scalability. In terms of additional passive component required, sensitivity of the circuit performance in the control scheme and control complexity the non-resonant DABs have an advantage over the SR DABs. However, SR DABs have a higher number of soft-switched (zero voltage and zero current switching) MOSFETs and near sinusoidal transformer currents, which result in lower switching and conduction losses. These positive performance impact factors of SR DABs outweigh their challenges for the considered application and operating conditions. In terms of efficiency and SiC MOSFET losses, the series-resonant variants outperform the non-resonant DABs with the SR ISOP FB DAB exhibiting the best performance. When the normalized cost and the VA ratings of SiC MOSFETs are considered, the ANPC DAB configuration seems to be the most promising one. Considering a fair trade-off between efficiency, loss distribution, VA ratings and the normalized cost, the SR ANPC DAB exhibits the best performance for this application.

7. References

[1] N. Matanov and A. Zahov, "Developments and Challenges for Electric Vehicle Charging Infrastructure," in *2020 12th Electrical Engineering Faculty Conference (BulEF)*, Sep. 2020, pp. 1–5. doi: 10.1109/BulEF51036.2020.9326080.

[2] R. W. A. A. De Doncker, D. M. Divan, and M. H. Kheraluwala, "A three-phase soft-switched high-power-density DC/DC converter for high-power applications," *IEEE Transactions on Industry Applications*, vol. 27, no. 1, pp. 63–73, Jan. 1991, doi: 10.1109/28.67533.

[3] B. Zhao, Q. Song, W. Liu, and Y. Sun, "Overview of Dual-Active-Bridge Isolated Bidirectional DC–DC Converter for High-Frequency-Link Power-Conversion System," *IEEE Transactions on Power Electronics*, vol. 29, no. 8, pp. 4091–4106, Aug. 2014, doi: 10.1109/TPEL.2013.2289913.

[4] J. Rabkowski, D. Peftitsis, and H.-P. Nee, "Silicon Carbide Power Transistors: A New Era in Power Electronics Is Initiated," *IEEE Industrial Electronics Magazine*, vol. 6, no. 2, pp. 17–26, Jun. 2012, doi: 10.1109/MIE.2012.2193291.

[5] J. Biela, M. Schweizer, S. Waffler, and J. W. Kolar, "SiC versus Si—Evaluation of Potentials for Performance Improvement of Inverter and DC–DC Converter Systems by SiC Power Semiconductors," *IEEE Transactions on Industrial Electronics*, vol. 58, no. 7, pp. 2872–2882, Jul. 2011, doi: 10.1109/TIE.2010.2072896.

[6] B. Whitaker *et al.*, "A High-Density, High-Efficiency, Isolated On-Board Vehicle Battery Charger Utilizing Silicon Carbide Power Devices," *IEEE Transactions on Power Electronics*, vol. 29, no. 5, pp. 2606–2617, May 2014, doi: 10.1109/TPEL.2013.2279950.

[7] D. Yıldırım, S. Ozturk, I. Cadirci, and M. Ermis, "All SiC PWM Rectifier Based Off-Board Ultrafast Charger for Heavy Electric Vehicles," *IET Power Electronics*, vol. 13, Aug. 2019, doi: 10.1049/iet-pel.2019.0583.

[8] X. Liang, S. Srdic, J. Won, E. Aponte, K. Booth, and S. Lukic, "A 12.47 kV Medium Voltage Input 350 kW EV Fast Charger using 10 kV SiC MOSFET," in *2019 IEEE Applied Power Electronics Conference and Exposition (APEC)*, Mar. 2019, pp. 581–587. doi: 10.1109/APEC.2019.8722239.

[9] Y. Du, X. Zhou, S. Bai, S. Lukic, and A. Huang, "Review of non-isolated bi-directional DC-DC converters for plug-in hybrid electric vehicle charge station application at municipal parking decks," in *2010 Twenty-Fifth Annual IEEE Applied Power Electronics Conference and Exposition (APEC)*, Feb. 2010, pp. 1145–1151. doi: 10.1109/APEC.2010.5433359.

[10] P. J. Grbović, P. Delarue, P. Le Moigne, and P. Bartholomeus, "A Bidirectional Three-Level DC–DC Converter for the Ultracapacitor Applications," *IEEE Transactions on Industrial Electronics*, vol. 57, no. 10, pp. 3415–3430, Oct. 2010, doi: 10.1109/TIE.2009.2038338.

[11] S. Rivera, B. Wu, S. Kouro, V. Yaramasu, and J. Wang, "Electric Vehicle Charging Station Using a Neutral Point Clamped Converter With Bipolar DC Bus," *IEEE Transactions on Industrial Electronics*, vol. 62, no. 4, pp. 1999–2009, Apr. 2015, doi: 10.1109/TIE.2014.2348937.

[12] M. Alharbi, M. Dahidah, V. Pickert, and J. Yu, "Comparison of SiC-based DC-DC modular converters for EV fast DC chargers," in *2019 IEEE International Conference on Industrial Technology (ICIT)*, Feb. 2019, pp. 1681–1688. doi: 10.1109/ICIT.2019.8843693.

[13] N. Keshmiri, M. I. Hassan, R. Rodriguez, and A. Emadi, "Comparison of Isolated Bidirectional DC/DC Converters Using WBG Devices for More Electric Aircraft," *IEEE Open Journal of the Industrial Electronics Society*, pp. 1–1, 2021, doi: 10.1109/OJIES.2021.3058196.

[14] M. Parvez, A. T. Pereira, N. Ertugrul, N. H. E. Weste, D. Abbott, and S. F. Al-Sarawi, "Wide Bandgap DC–DC Converter Topologies for Power Applications," *Proceedings of the IEEE*, vol. 109, no. 7, pp. 1253–1275, Jul. 2021, doi: 10.1109/JPROC.2021.3072170.

[15] Y. V. Pushpalatha and D. Peftitsis, "Design of Dual Active Bridge Converters with SiC MOSFETs for minimized reflow power operation," in *2021 IEEE 12th Energy Conversion Congress & Exposition - Asia (ECCE-Asia)*, Singapore, Singapore, May 2021, pp. 574–579. doi: 10.1109/ECCE-Asia49820.2021.9479059.

[16] Xiaodong Li and A. K. S. Bhat, "Analysis and Design of High-Frequency Isolated Dual-Bridge Series Resonant DC/DC Converter," *IEEE Trans. Power Electron.*, vol. 25, no. 4, pp. 850–862, Apr. 2010, doi: 10.1109/TPEL.2009.2034662.